



Molecular beam deposition of high-permittivity polydimethylsiloxane for nanometer-thin elastomer films in dielectric actuators



Florian M. Weiss^a, Frederikke B. Madsen^b, Tino Töpfer^a, Bekim Osmani^a, Vanessa Leung^a, Bert Müller^{a,*}

^a Biomaterials Science Center, Department of Biomedical Engineering, University of Basel, Gewerbestrasse 14, 4123 Allschwil, Switzerland

^b Danish Polymer Centre, Department of Chemical and Biochemical Engineering, Technical University of Denmark, DTU, Søtofts Plads, Bldg. 227, 2800 Kgs. Lyngby, Denmark

ARTICLE INFO

Article history:

Received 12 February 2016

Received in revised form 11 May 2016

Accepted 13 May 2016

Available online 16 May 2016

Keywords:

Dielectric elastomer actuator

Chloropropyl-functional

Vinyl-terminated siloxane co-oligomer

Thermal evaporation

Ultra-violet light curing

Atomic force microscopy

Indentation test

Surface roughness

Spectroscopic ellipsometer

ABSTRACT

To realize low-voltage dielectric elastomer actuators (DEAs) for artificial muscles, a high-permittivity elastomer and a related thin-film deposition technique must be selected. For polydimethylsiloxane, fillers or functionalized crosslinkers have been incorporated into the elastomer to improve dielectric properties. To produce elastomer layers nanometers thin, molecular beam deposition was introduced. We pursue the synthesis of a high-permittivity oligomer, namely a chloropropyl-functional, vinyl-terminated siloxane to be thermally evaporated and subsequent UV curing to form an elastomer. The synthesized oligomer exhibits dielectric permittivity enhanced by 33% and a breakdown increase of 26% with respect to the commercially available oligomer DMS-V05. Films 160 nm thin were fabricated after being evaporated under ultra-high vacuum conditions. Spectroscopic ellipsometry served for film growth monitoring. Using atomic force microscopy, the film surface morphology and mechanics were characterized after growth termination and subsequent curing. The Young's modulus of the elastomer corresponded to (1.8 ± 0.2) MPa and is thus a factor of two lower than that of DMS-V05. Consequently, the properties of the films prepared by the new elastomer can be quantified by the normalized figure of merit, which estimates to 4.6. The presented approach is an essential step toward the realization of low-voltage DEA for medical applications and beyond.

© 2016 Elsevier Ltd. All rights reserved.

1. Introduction

Dielectric elastomer actuators (DEAs) have found a number of applications in tactile displays [1–3], adaptable lenses and gratings [4], sound systems [5], (bio-mimicking) robotics [6–8], and sensors [9,10]. They are well established in research but currently require driving voltages well above 100 V, which makes them unsuitable for use in areas such as medical implants. To expand their potential, a great number of attempts have been made to decrease operating voltages. The most common approach to date in this regard involves enhancing the dielectric properties of the elastomeric material through the use of composite systems or by chemical modification. An alternative, physics-based approach is to reduce the thickness of the elastomer layer to the sub-micrometer level. The resulting ultrathin DEA layers are stacked to provide the required force.

Composite systems containing fillers such as TiO₂ [11,12], BaTiO₃ [13–15], and Al₂O₃ [16] are used to increase the dielectric permittivity of silicone elastomers. Other conducting fillers such as expanded graphite [17], carbon nanotubes [18,19], and encapsulated conducting polymers [20,21] have also been employed. Such composite systems,

however, have the drawback that increased dielectric permittivity is often accompanied by an increased Young's modulus, which in turn reduces achievable strain. Furthermore, composite systems may experience large dielectric losses and reduced breakdown strength, as increases in dielectric permittivity are achieved at loadings near the percolation threshold. Systems near the percolation threshold are prone to filler agglomeration and consequently significant changes in local mechanical properties.

Chemical silicone modifications have been used to create silicone elastomers with increased permittivity, and they lead to a more controlled network structure than composite systems, which depends on the mixing of particles. Furthermore, no free species are present in the networks. Several approaches have been followed to create chemically-modified silicone elastomers with high permittivity. Kussmaul et al. [22], for example, added the synthesized dipolar molecule *N*-allyl-*N*-methyl-*p*-nitroaniline, together with compensating amounts of a hydride-functional cross-linker, to a silicone matrix. Soft silicone elastomers with high permittivity were also prepared by Racles et al. [23], who used cyanopropyl-functional silicones to raise dielectric permittivity, while Madsen et al. used nitrobenzene- and azonitrobenzene-functional cross-linkers [24] and copolymers [25,26]. Very recently, Madsen et al. [27] demonstrated the synthesis and use of chloropropyl-functional, vinyl-terminated siloxane copolymers. The resulting elastomers

* Corresponding author.

E-mail address: bert.mueller@unibas.ch (B. Müller).

were demonstrated to be soft, have a permittivity ϵ' up to 4.7, high breakdown strength, and, very importantly, equally low dielectric loss as the PDMS reference material.

An alternative to changing dielectric properties is lowering the operation voltage by applying thin elastomer layers. As a decrease in thickness leads to a quadratic decrease in the driving voltage required for a given strain, even a small thickness reduction leads to a large payoff. Using molecular beam deposition (MBD), elastomeric polydimethylsiloxane (PDMS) was deposited with film thicknesses in the range of 200 nm [28]. The PDMS thin films could be driven at voltages well below 40 V, marking a promising step forward toward a low-voltage DEA.

Combining elastomers with improved dielectric permittivity with thin-film fabrication in the sub-micrometer range promises to lower the operating voltage more effectively than either of these two approaches can achieve alone. Implementing this combined approach requires a material (i) with high permittivity compared to pure PDMS and (ii) which can be deposited by evaporation under high-vacuum conditions.

Composite systems are inappropriate for fabricating nanometer-thin films *via* MBD for two reasons. First, there is a high risk of aggregation and imperfections, which will severely influence mechanical and breakdown properties. Second, it is impossible to fabricate films from composite systems by evaporation. Furthermore, as the fabrication of nanometer-thin films by evaporation requires low molecular weight oligomers, materials with bulky and heavy dipolar groups must also be ruled out.

Ideally, the structure of the high-permittivity oligomer should be similar to pure PDMS, since the pure oligomer has previously been deposited successfully by evaporation. Furthermore, it should be possible to produce specific molecular weights of the high-permittivity oligomer, since at a given temperature only oligomers within a narrow molecular weight range can be evaporated. The chloropropyl-functional, vinyl-terminated siloxane copolymers recently synthesized by Madsen et al. [26,27] would satisfy the requirements for application as a high-permittivity nanometer-thin silicone elastomer, provided that their molecular weight can be tailored to the needs of MBD.

In this work we report that we have obtained chloropropyl-functional, vinyl-terminated siloxane co-oligomer with specific molecular weights that are in a suitable range for MBD. Two of these oligomers were characterized and deposited by thermal evaporation under ultra-high vacuum (UHV) conditions. Their film growth was monitored and characterized using *in situ* spectroscopic ellipsometry (SE). Additionally, nanometer-thin films were cured by ultraviolet (UV) radiation, and the resulting films were analyzed using atomic force microscopy (AFM) for nano-indentation and topological measurements.

2. Experimental

2.1. Materials

3-Chloropropylmethylmethoxysilane, 1,1,3,3,5,5-hexamethyltrisiloxane, dimethoxydimethylsilane, vinyltrimethylsilane, and DMS-V05 were purchased from Gelest Inc. All other chemicals were acquired from Sigma-Aldrich and used as received, unless otherwise stated.

2.2. Synthesis of α,ω -vinyl-poly((chloropropyl)methylsiloxane-co-dimethylsiloxane) (CI-PDMS)

The synthesis was adapted from a previously described procedure [26] using 3-chloropropylmethylmethoxysilane (10.00 g, 54.7 mmol) which was dissolved in dry heptane (200 mL) in a 2 L two-neck round-bottomed flask. 1,1,3,3,5,5-hexamethyltrisiloxane (9.36 g, 44.9 mmol) was added, and the mixture was stirred for 5 min. Tris(pentafluorophenyl)borane (7 mL, 0.04 M, 0.2 mol%) in dry toluene

was added and methane gas developed. The mixture was then stirred at room temperature for 1 h, and thereafter excess dimethoxydimethylsilane (23.8 g, 198 mmol) was added in order to quench any potentially remaining hydride groups and to ensure that all oligomers possessed methoxy end groups. The reaction mixture was stirred additionally for a couple of hours. The solvent and excess dimethoxydimethylsilane (bp: 82 °C) were removed *in vacuo* at a temperature of 45 °C with toluene, to make the product a clear oil. The product was thereafter re-dissolved in heptane (75 mL), vinyltrimethylsilane (40 g, 464 mmol) was added, and the mixture was then stirred overnight, after which ¹H NMR was used in order to confirm the removal of methoxy groups and conversion to vinyl groups. Neutral aluminum oxide (20 g) was added to the reaction mixture to remove the tris(pentafluorophenyl)borane catalyst, and the solution was then filtered. The solvent and excess vinyltrimethylsilane reagents were removed *in vacuo*, to make the product a clear oil (16.02 g, 91%). SEC (Toluene): $M_n = 791$ g/mol, $M_w = 1116$ g/mol. IR measurements provided the following vibration modes (wave numbers): 3050 cm^{-1} for the Si–CH=CH₂ stretch, 2960 cm^{-1} for the C–H stretch, 1600 cm^{-1} for the Si–CH=CH₂ stretch, 1410 cm^{-1} for the Si–CH₂ and Si–CH=CH₂ stretches, 1260 cm^{-1} for the Si–CH₃ stretch, and 1055 cm^{-1} for the Si–O stretch. ¹H NMR (CDCl₃, δ_H , ppm): 0.08–0.1 (m, ~80H, CH₃–Si), 0.65 (m, ~8H, –Si–CH₂–CH₂–), 1.82 (m, ~8H, –CH₂–CH₂–CH₂), 3.50 (t, ~8H, ³J = 6.9 Hz, Cl–CH₂–CH₂). 5.73 (dd, 2H, ²J = 4.2 Hz, ³J = 20 Hz, CH=CH₂), 5.94 (dd, 2H, ²J = 4.2 Hz, ³J = 15 Hz, CH=CH₂), 6.12 (dd, 2H, ³J = 15 Hz, ³J = 20 Hz, –CH=CH₂). ¹³C NMR (CDCl₃, δ_C , ppm): –0.75 to 1.08 (c + d + h), 15.67 (e), 26.71 (f), 47.59 (g), 131.86 (a), 139.10 (b).

2.3. Characterization of DMS-V05 and CI-PDMS

Fourier transform infrared (FTIR) spectroscopy was performed on a Thermo Scientific iS50 equipped with a diamond crystal attenuated total reflection (ATR) sampling accessory. Spectra were recorded in the range of 4000 to 400 cm^{-1} . ¹H and ¹³C NMR experiments were performed on a Bruker 300 MHz spectrometer in CDCl₃, while size-exclusion chromatography (SEC) was performed on a Tosoh EcoSEC HLC-8320GPC instrument equipped with IR and UV detectors and SDV Linear S columns from PSS. Samples were run in toluene at a temperature of 35 °C at a rate of 1 mL min^{–1}, and molar mass characteristics were calculated using WinGPC Unity 7.4.0 software and linear PDMS standards acquired from PSS. Thermal gravimetric analysis (TGA) was performed on a TA Discovery TGA from TA Instruments, and measurements were carried out in a nitrogen atmosphere at a heating rate of 10 K min^{–1}, from room temperature to 800 °C, while differential scanning calorimetry (DSC) measurements were performed on a TA Discovery DSC from TA Instruments. The DSC thermal analyses were performed at a heating and cooling rate of 10 K min^{–1} from –150 to 200 °C. Dielectric relaxation spectroscopy (DRS) was performed on a Novocontrol Alpha-A high-performance frequency analyzer (Novocontrol Technologies GmbH & Co) operating in the frequency range 10² to 10⁷ Hz at room temperature. The liquid oligomer samples were added to a Teflon ring with a diameter of 25 mm, which was attached to a bottom electrode. Dielectric breakdown strengths were measured on an in-house-built device based on international standards. The liquid oligomers DMS-V05 and CI-PDMS were dropped into a Teflon ring, which was mounted on the bottom spherical electrode. The top spherical electrode was then adjusted to a distance of 100 μm between the electrodes, and a stepwise increasing voltage was applied until breakdown was observed in the form of a spark and noise between the electrodes. After the breakdown a black breakdown point was seen within the sample.

2.4. Nanometer-thin film preparation by MBD

The PDMS thin films were thermally evaporated and deposited under ultra-high vacuum conditions. The base pressure in the chamber

was 10^{-9} mbar, and the oligomers DMS-V05 and CI-PDMS were filled in a crucible without any purification and then evaporated using low-temperature effusion cells (NTEZ, Dr. Eberl MBE Komponenten GmbH, Weil der Stadt, Germany) with a 25 cm^3 crucible for DMS-V05 and a 2 cm^3 crucible for CI-PDMS. DMS-V05 was evaporated at a crucible temperature of 130°C and CI-PDMS at a temperature of 199°C . As substrates, 2-in. n-doped Si-wafers (SIEGERT WAFER GmbH, Aachen, Germany) with a thickness of $(279 \pm 25) \mu\text{m}$ were used. They were rotated at a speed of 1.2 rpm and a distance of 30 mm at room temperature. The films were cured during and after deposition by exposing them to UV radiation from an externally mounted source (H2D2 light source L11798, Hamamatsu, Japan) through a CaF window for a period of 20 h 50 min.

2.5. Real-time spectroscopic ellipsometry

To examine real-time deposition, a spectroscopic ellipsometer (SE801, Sentech, Berlin, Germany) with SpectraRay3 software was used. The detected spectrum, monitored at a frequency of 1 Hz and an incident angle of 70° , ranged from 190 to 1050 nm, and an incident beam diameter of 4 mm resulted in a measurement spot of $4 \times 10 \text{ mm}^2$. The obtained wavelength-dependent Ψ and Δ values, or the Fourier coefficients S1 and S2, are related to the complex Fresnel reflection coefficients r_p and r_s of p (parallel) and s (perpendicular) polarized light and their ratio ρ by

$$\rho = r_p/r_s = \tan\Psi \cdot e^{i\Delta}. \quad (1)$$

With the obtained Fresnel reflection coefficient ratio it is possible to extract the wavelength-dependent dielectric function $\tilde{n}(\lambda)$

$$\langle \tilde{n} \rangle^2 = \langle (n) + i(k) \rangle^2 = \sin^2(\phi_0) \cdot \left(1 + \tan^2(\phi_0) \left(\frac{1-\rho}{1+\rho} \right)^2 \right). \quad (2)$$

where ϕ_0 represents the angle of the incident beam, $n(\lambda)$ the real and $k(\lambda)$ the imaginary parts of the refractive index, respectively. To determine the linear and first-order non-linear refractive index of DMS-V05 and CI-PDMS a measurement of a spin-coated, 150 nm-thick film of each oligomer was conducted and resulted in $n_0 = 1.384 \pm 0.001$, $n_1 = 22.3 \pm 0.1$, $n_2 = 24.7 \pm 0.1$ for DMS-V05 and $n_0 = 1.418 \pm 0.001$, $n_1 = 22.3 \pm 0.1$, and $n_2 = 20.0 \pm 0.1$ for the CI-PDMS. These values were approximated using the Cauchy series of the refractive index $n(\lambda) = n_0 + c_1 n_1/\lambda^2 + c_2 n_2/\lambda^4$ with $c_1 = 10^2 \text{ nm}^2$ and $c_2 = 10^4 \text{ nm}^2$, whereas the extinction coefficient k was kept at zero.

To determine the growth mechanism, a Cauchy layer and an effective medium approximation (EMA) model were applied. The Cauchy layer model represents the simplest approach and assumes a perfect plane parallel surface and two-dimensional growth. Bruggeman's EMA model [29] includes surface roughness induced by the nucleation centers. The uppermost layer, consisting of clusters and voids (or inclusions), is considered as having an effective dielectric or optical property deduced from equal fractional parts of the deposited and void material, cf. Eq. (3) below.

$$0 = \sum_{i=1}^N f_i \frac{n_i^2 - n_e^2}{n_i^2 + 2n_e^2}. \quad (3)$$

Table 1

Number average molecular weights M_n and weight average molecular weights M_w , obtained by SEC for the different fractions of the thermally evaporated DMS-V05 under ultra-high vacuum conditions.

	DMS-V05 (original)	DMS-V05 (residue)	DMS-V05 (deposited)
M_n	807 g/mol	1560 g/mol	944 g/mol
M_w	1364 g/mol	1910 g/mol	1033 g/mol

Table 2

SEC results of CI-PDMS and DMS-V05 for comparison.

	DMS-V05 (deposited)	CI-PDMS
M_n	944 g/mol	791 g/mol
M_w	1033 g/mol	1116 g/mol

The EMA is only applicable if the measured system fulfills two key assumptions: (i) The surface roughness/nucleation centers are smaller than the minimum wavelength, in order to ignore light scattering, and (ii) dielectric function has to be size- and shape-independent. For the thermally evaporated PDMS, both of these key points were fulfilled. For the evaluation of the data the void fraction was set to 0.5, which is reasonable according to Fujiwara et al. [30].

For the evaluation of the models the mean square error (MSE) of the divergence from the obtained fit to the acquired data was compared. The MSE is defined in Eq. (4).

$$\text{MSE} = \frac{1}{N} \sqrt{\sum_{i=1}^N \left\{ \left(\frac{\Psi_i^m - \Psi_i^{th}}{\delta\Psi} \right)^2 + \left(\frac{\Delta_i^m - \Delta_i^{th}}{\delta\Psi} \right)^2 \right\}} \quad (4)$$

2.6. Atomic force microscopy

The mechanical properties of the evaporated and UV cross-linked polymer structures were assessed using AFM spectroscopic methods (FlexAFM C3000, Nanosurf AG, Switzerland). Here, 900 indentation measurements on $30 \mu\text{m} \times 30 \mu\text{m}$ arrays were acquired at loads of 25 and 10 nN, using a soft cantilever with a spherical tip ($R = 150 \text{ nm}$, B150_CONTR, Nanotools GmbH, Germany). Calculations were based on the Johnson-Kendall-Roberts (JKR) model of elastic contact theory incorporating adhesion effects. The software employed in this instance was developed by Nanosurf AG (FLEX-ANA®, Automated Nanomechanical Analysis) to perform calculations for each force distance curve. Potential effects of the Si substrate were neglected, since the indentation depths were below 50 nm.

Surface topology measurements ($5 \times 5 \mu\text{m}^2$, tapping mode, vibration amplitude 370 mV (DMS-V05), and a 1.22 V (CI-PDMS) set point 5%) were performed using a FlexAFM System (Nanosurf AG, Liestal, Switzerland). In total, 1024 lines at speeds of 0.982 s (DMS-V05) and 4.94 s (CI-PDMS) were acquired for each image, using a non-contact soft tapping AFM probe (Tap190Al-G probe, NanoAndMore GmbH, Wetzlar, Germany). The root-mean-squares of the surface values were calculated using Gwyddion 2.41 software (Gwyddion: Open-source software for SPM data analysis, <http://gwyddion.net>).

3. Results and discussion

3.1. Oligomer characterization and comparison

The molecular weight characteristics of DMS-V05 were obtained using size exclusion chromatography (SEC). The oligomer DMS-V05, as purchased, was evaporated under UHV conditions as stated in Section 2.4. Subsequently, the deposited material and the residue in the crucible were harvested for SEC. The experimental data for the molecular weights of these three species are listed in Table 1.

Table 3

Dielectric breakdown strengths of the liquid oligomers DMS-V05 and CI-PDMS.

	Thickness (μm)	Voltage at breakdown (kV)	Breakdown strength (V/ μm)
DMS-V05	100	1.01 ± 0.03	10.1 ± 0.3
CI-PDMS	100	1.27 ± 0.05	12.7 ± 0.5

Table 4
Summary of properties of DMS-V05 and Cl-PDMS as well as figure of merit calculations.

	Dielectric permittivity	Breakdown strength	Young's modulus	Normalized figure of merit
	ϵ'	E_B (V/ μm)	Y (MPa)	F_{om}/F_{om_ref}
DMS-V05	3	10.1 \pm 0.3	3.9 \pm 0.3	1
Cl-PDMS	4	12.7 \pm 0.5	1.8 \pm 0.2	4.6

Knowing the weight properties of the commercially available 'standard' oligomer, the target molecular weight should be in the same range as the deposited PDMS. Hence, a siloxane co-oligomer with dielectric permittivity-enhancing chloropropyl groups was synthesized according to the described procedure [26], though this was modified to create a low-molecular weight co-oligomer. The co-oligomer was prepared from commercially available starting materials through the tris(pentafluorophenyl)borane-catalysed Piers-Rubinsztajn condensation reaction of 3-chloropropylmethylmethoxysilane and the hydride-terminated dimethylsiloxane molecule 1,1,3,3,5,5-hexamethyltrisiloxane, which constituted the spacer unit between the functional chloropropyl groups. The chosen quantities of the precursors resulted in co-oligomers containing approximately four chloropropyl-functional groups. The co-oligomer was then end-functionalized with vinyl groups to allow for UV-initiated cross-linking reactions. The structure and reactive pathway for the resulting co-oligomer, α,ω -vinylpoly((chloropropyl)methylsiloxane-co-dimethylsiloxane) (Cl-PDMS), can be seen in Scheme 1.

The aim of the synthesis from a molecular weight point of view was to achieve a molecular weight in the range of 'DMS-V05 deposited', cf. Table 1, since this is the molecular weight that is actually evaporated during sample preparation. As seen in Table 2, oligomer Cl-PDMS has a molecular weight comparable to 'DMS-V05 deposited', albeit a slightly higher polydispersity index.

The prepared co-oligomer, Cl-PDMS, as well as the commercial oligomer, DMS-V05, were characterized with FTIR and ^1H and ^{13}C NMR. FTIR spectra can be found as supporting information, and, as expected, there are no major differences between DMS-V05 and Cl-PDMS in their FTIR spectra. Peaks associated to the chloropropyl group are very weak but can be observed at frequencies of 1310 and 910 cm^{-1} whereas the one at 860 cm^{-1} is invisible due the overlap of the strong peak from the Si-CH₃ absorption [31]. The results of ^1H NMR measurements of Cl-PDMS are summarized in the experimental section. The ^1H NMR spectra of both Cl-PDMS and DMS-V05 are furthermore given as supporting information. It is clear that Cl-PDMS is structurally different from DMS-V05. Both oligomers possess peaks for Si-CH₃ protons at $\delta_{\text{H}} = 0.08$ –0.1 ppm as well as $-\text{CH}=\text{CH}_2$ protons in the form of three distinctive doublets of doublets at $\delta_{\text{H}} = 5.7$ –6.1 ppm. The Cl-PDMS oligomers conversely have three distinctive multiplets, representing the protons from each of the $-\text{CH}_2-$ groups in the chloropropyl-functionality at $\delta_{\text{H}} = 0.65$, 1.82 and 3.50 ppm, respectively. ^{13}C NMR corroborated these results for Cl-PDMS through resonances at $\delta_{\text{C}} = 15.67$, 26.71 and 47.59 ppm, for the $-\text{CH}_2-$ carbon atoms in the propyl-chain, and resonances at $\delta_{\text{C}} = 131.86$ and 139.10 ppm for the two carbon atoms in the vinyl groups ($-\text{CH}=\text{CH}_2$).

The effect of molecular structure on the thermal behavior of the two oligomers was measured by DSC. The measured thermograms are presented in the supporting information. Both DMS-V05 and Cl-PDMS

show glass transition temperatures T_g well below -100 °C, which is characteristic for siloxanes. None of the oligomers exhibit a clear crystallization temperature T_c , but DMS-V05 does show a small melting peak T_m . For Cl-PDMS, no T_c or T_m is observed, which means that the oligomer does not crystallize. This behavior points to the successful formation of spatially well-separated chloropropyl-functional groups along the oligomer backbone.

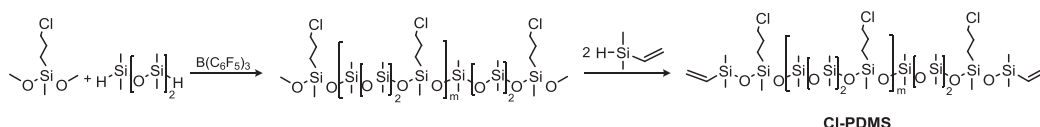
The thermal behavior and stability of the oligomers DMS-V05 and Cl-PDMS was measured with TGA. As seen in the thermogram, evaporation for Cl-PDMS starts at a lower temperature than for DMS-V05, which may be due to a larger fraction of small molecules such as residual solvent, starting materials, and smaller oligomers. After this initial evaporation, oligomer evaporation starts at approximately 150 °C, which is comparable to DMS-V05. Polysiloxanes are known for their thermal stability. Decomposition phenomena, however, cannot be ruled out. As clear from Fig. 1, the degradation of higher molecular weight fractions starts at temperatures well above 300 °C.

Dielectric permittivity of Cl-PDMS oligomer was measured by dielectric relaxation spectroscopy, and the results are shown in the supporting information. At a frequency of 100 Hz the Cl-PDMS oligomer gives rise to $\epsilon' = 4.0$ and DMS-V05 to $\epsilon' = 3.0$, which is a 33% increase in permittivity. Furthermore, dielectric losses remain relatively low for the Cl-PDMS oligomer.

It was impossible to measure the dielectric breakdown strength of cured samples, using traditional methods [32], due to the nanometer-sized thicknesses of the films, which makes handling too difficult. Furthermore, measured breakdown strength depends strongly on the elastomer's film thickness [33,34]. Instead, the breakdown strengths of the liquid, low-viscosity oligomers, DMS-V05 and Cl-PDMS, were measured. The results are presented in Table 3. It can be seen that the dielectric breakdown strength of Cl-PDMS is approximately 25% higher than that for DMS-V05. Since the measurements were performed on liquid samples, there is no dependency regarding the stiffness of the samples, which is observed for elastomers [35–37]. Here, the breakdown strength has been found to scale linearly – or even exponentially – with the Young's modulus. Therefore, the results give a clear indication that the breakdown strength of Cl-PDMS in the cured state would also be higher than that of DMS-V05 in the cured state at comparable Young's moduli.

3.2. Nanometer-thin film deposition

During deposition under UHV conditions spectroscopic ellipsometry data was acquired, in order to characterize the island and film growth of the oligomers. The successful evaluation of the data, using the Cauchy layer (CL) and the effective medium approximation (EMA), as introduced by Bruggeman, is shown in Fig. 2, where the diagrams in (a) and (b) represent the oligomer layer thicknesses derived from the CL model for DMS-V05 and Cl-PDMS, respectively. Diagrams (c) and (d) show EMA layer thicknesses, which are plotted against the deposition time. The time scales differ by a factor of ten. Obviously, the oligomers grow according to the CL model, and during the initial stages of deposition the films grow relatively quickly. The point of inflection, related to the maximal deposition rate, is already reached between 10 and 20 nm, following which deposition time eventually decreases. Applying the EMA model and considering surface roughness, the data reveal that for DMS-V05 the surface is intrinsically flat, thus indicating two-dimensional growth. During the initial growth stages of Cl-PDMS, EMA layer



Scheme 1. Synthetic route for chloropropyl-functional siloxane co-oligomer Cl-PDMS.

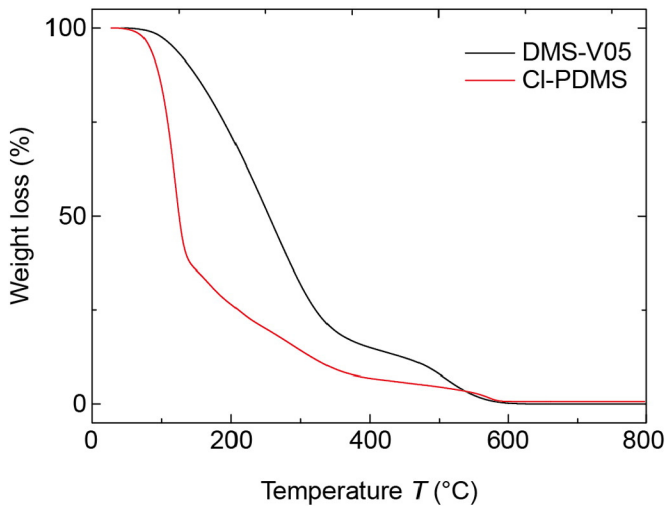


Fig. 1. TGA thermograms of DMS-V05 and Cl-PDMS. The Cl-PDMS shows a first shoulder at a temperature of 140 °C attributed to the loss of precursor and solvent molecules. For both oligomers a shoulder is observed at a temperature of about 350 °C, being a known value for the decomposition of dimethylsiloxane fluids.

thickness seems to fluctuate around a mean value of about 2.5 nm. A maximum EMA thickness of 12 nm is reached at 4800 s, thereby indicating that up to this time three-dimensional growth dominates. Subsequently, film growth switches to the layer-by-layer mode.

The observed three-dimensional growth during the early stages of Cl-PDMS deposition is attributed to the increased polarity of the chloropropyl side chains, as a result of which wettability seems to decrease and therefore islands form. This polarity increase also explains the relatively high evaporation temperature related to the slow deposition rate, which is due to stronger interactions between the molecules. Another source for the deposition rate difference is the crucible size, in

that the larger the crucible, the larger its surface and the related number of molecules that evaporate.

After DMS-V05 deposition the UV curing was continued. During this treatment, the parameters S1 and S2 were monitored to detect the associated changes of the film properties. After a period of 21 h the parameters S1 and S2 continuously acquired could be considered as constant. This behavior was interpreted as termination of the curing process.

3.3. Comparison of UV-cured DMS-V05 and Cl-PDMS

Comparing the wavelength-dependent refractive indices of DMS-V05 and Cl-PDMS, before and after post-deposition curing, see Fig. 3, two observations arise. First, the refractive index of Cl-PDMS exceeds the one of DMS-V05. Second, curing increases the refractive indices of the two oligomers. In the case of DMS-V05 the increase is more pronounced. It is interesting to note that for Cl-PDMS one observes a slight ratio decrease in the refractive indices after-to-before curing in line with increasing wavelength, whereas for DMS-V05 it increases slightly.

The larger refractive index of Cl-PDMS with respect to DMS-V05 originates from the polarity of the chloropropyl-functional co-oligomer. This observation provides further evidence that Cl-PDMS has the higher dielectric permittivity, since the refractive index and permittivity are proportional, linked *via* the complex dielectric function. The increase in the refractive index, owing to cross-linking, is related to the curing reaction mechanism not being fully understood yet. During the UV irradiation, two mechanisms may occur simultaneously. First, IR spectroscopy showed a diminished concentration of the vinyl groups [28]. Second, it has been reported that high-energy radiation cleaves the Si–C and CH₂–H bonds [38]. The cleavage of the Si–C bond eventually induces the formation of SiO₂ [39]. Thus, the refractive index leans more toward SiO₂, which corresponds to 1.460 at 632 nm [40]. The greater increase in the refractive index of DMS-V05 is attributed to the higher number of methyl groups present compared to Cl-PDMS. This finding has been supported by Yahya et al. [41], who investigated the refractive index

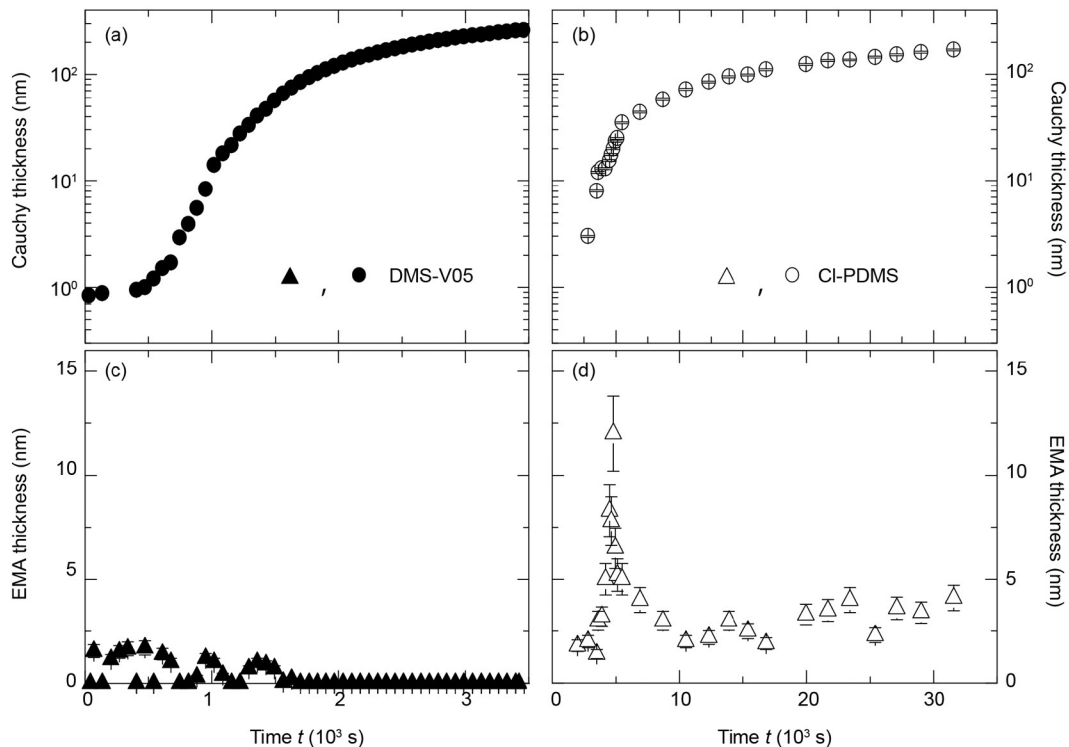


Fig. 2. Deposition data of DMS-V05 and Cl-PDMS acquired *in situ* by spectroscopic ellipsometry. Diagrams (a) DMS-V05 and (b) Cl-PDMS were obtained by applying the Cauchy model. The data in diagrams (c) DMS-V05 and (d) Cl-PDMS correspond to the effective medium approximation.

with respect to cross-link density. Interestingly the Si–C bond of the chloropropyl side chain tends to be more stable against the UV light than the methyl group. This behavior is indicated by the presence of chloride in the energy dispersive X-ray spectra of the film as well as by the FTIR measurements exhibiting the related absorption peak at 1310 cm^{-1} .

Nano indentation, obtained by atomic force microscopy, was not analyzed using the Hertz contact model, since the adhesion forces are in the range of the applied forces. Therefore, the Johnsons-Kandall-Robers model [42], which considers adhesion forces, was applied to evaluate force distance curves, with the goal of extracting the Young's moduli. Fig. 4 displays the histograms of the 900 indentation measurements performed on each polymer film. The indentation depth for DMS-V05 was $(26 \pm 1)\text{ nm}$ and for CI-PDMS $(38 \pm 2)\text{ nm}$. The Young's modulus of 160 nm-thin CI-PDMS films is a 2.2 factor lower than that of DMS-V05, as shown in Fig. 4. This result relates to the cross-link density of CI-PDMS, owing to the lower number of methyl groups and bulky side chains.

By measuring stiffness profiles from the center toward the rim of the substrate, one recognizes that the Young's modulus decreases. This behavior is understandable, because UV radiation determines the degree of curing. Furthermore, we observed a skin effect present at the intermediate curing stages. After indentation the AFM camera shows the impression crater, which vanishes over time. This viscoelastic behavior is presumably due to a liquid phase below the skin layer. As the curing starts from the surface, the formation of a skin layer at intermediate curing stages sounds reasonable.

Fig. 5 presents the characteristic force-distance curves of the nano-indentation measurements. Pull-off force, also termed adhesion force, $F_{adh2} = (20.5 \pm 0.3)\text{ nN}$ for CI-PDMS is slightly greater than adhesion force $F_{adh1} = (17.7 \pm 0.2)\text{ nN}$ for DMS-V05. The area below the zero force of retracting curves generally corresponds to the adhesion works W_{adh1} and W_{adh2} describing the energy the cantilever has to overcome to get back into the zero-force regime. The work of adhesion W_{adh} per unit area for a spherical tip on a flat surface, according to the JKR model, can be calculated from the tip radius R [43]:

$$W_{adh} = \frac{2F_{adh}}{3\pi R} \quad (5)$$

Adhesion force depends on material properties and on surface roughness [43]. AFM measurements allow for determining surface roughness $S_q = (0.898 \pm 0.001)\text{ nm}$ for CI-PDMS and (0.425 ± 0.001)

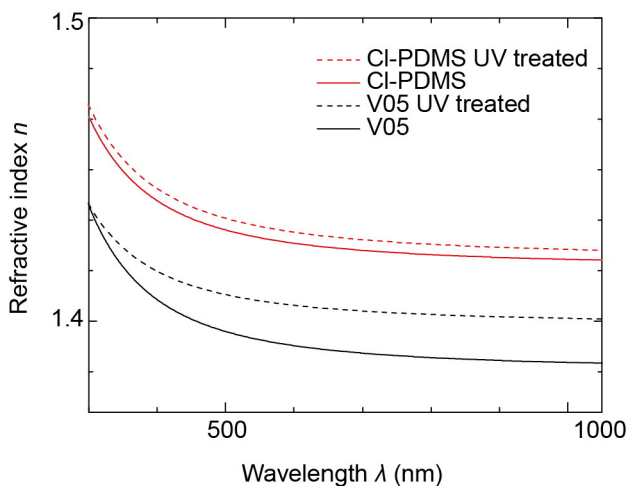


Fig. 3. Refractive indices of DMS-V05 (black) and CI-PDMS (red) measured by means of spectroscopic ellipsometry. The solid lines represent data obtained after deposition, and the dotted lines values after UV curing. (For interpretation of the references to color in this figure legend, the reader is referred to the web version of this article.)

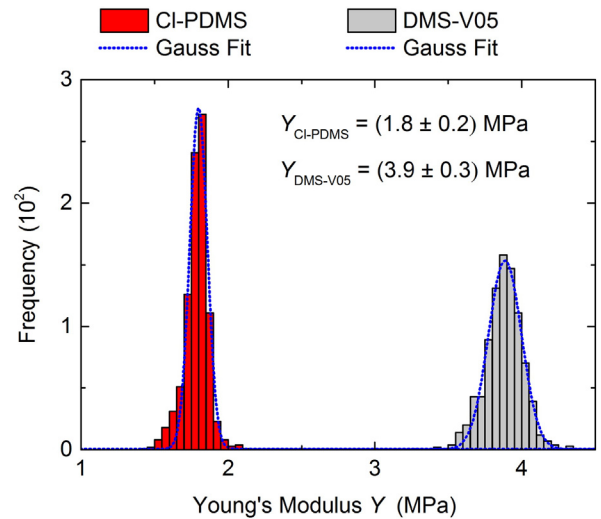


Fig. 4. Young's modulus of cured DMS-V05, in grey, and CI-PDMS, in red, measured by AFM nano-indentation. Both samples have a thickness of 160 nm and were UV irradiated for 20 h and 50 min. (For interpretation of the references to color in this figure legend, the reader is referred to the web version of this article.)

nm for DMS-V05. Differences in surface roughness, cf. Fig. 6, give rise to the value of $W_{adh}(\text{CI-PDMS}) = 29\text{ mJ/m}^2$ compared to $W_{adh}(\text{DMS-V05}) = 25\text{ mJ/m}^2$, as described by the adhesion observed on artificially roughened PDMS surfaces [44].

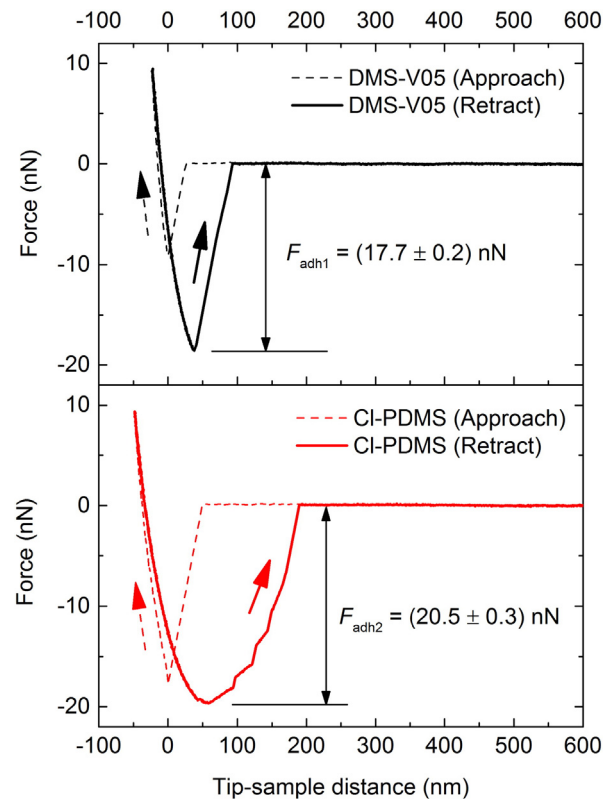


Fig. 5. Force–distance curves are converted from the deflection of the cantilever and the z-piezo position for the deposited and cured films. The black dashed and solid lines represent the approach and the retracting curves of DMS-V05, respectively, whereas the red lines are for CI-PDMS. Negative values indicate the indentation depth of the tip. The error for adhesion forces F_{adh1} and F_{adh2} corresponds to the standard deviation of the Gaussian fit applied to the adhesion histograms. (For interpretation of the references to color in this figure legend, the reader is referred to the web version of this article.)

The surface roughness of the cured films, derived from the AFM measurements and depicted in Fig. 6, mirrors the values found by the spectroscopic ellipsometry experiments presented in Section 3.2.

To compare dielectric elastomers, P. Sommer-Larsen and A. Ladegaard Larsen [45] defined a single parameter, namely the *figure of merit* F_{om} , which depends on the dielectric constant, dielectric breakdown strength, and the Young's modulus of the elastomer:

$$F_{om} = \frac{3\varepsilon' E_B^2}{Y}$$

The figure of merit is often normalized to a reference material. In the present communication, we take DMS-V05 as a reference and hence obtain 4.6 for CI-PDMS, cf. Table 4. As the figure of merit can be used to optimize elastomer properties for dielectric elastomer actuators [45], it demonstrates that CI-PDMS is a much better choice for fabricating low-voltage DEAs.

4. Conclusion

The chloropropyl-functional co-oligomer CI-PDMS can be synthesized with a molecular weight adapted for thermal evaporation under vacuum conditions. Therefore, it can be readily compared with the

commercially available oligomer DMS-V05. This choice supports the direct comparison with other starting materials for the preparation of polymer films for DEA applications. With a 33% increased dielectric constant and a greater than two-fold reduction in the Young's modulus, the used CI-PDMS is much better suited than the commercially available DMS-V05 for preparing nanometer-thin films for low-voltage DEAs.

The nanometer-thin polymer films are not only difficult to handle for characterization purposes, but need to be significantly improved to reach a defect level that enables their reliable use for the desired sensor and actuator applications.

Acknowledgements

The authors acknowledge helpful discussions with Anne Ladegaard Skov and the active support of Liyun Yu (dielectric spectroscopy and dielectric breakdown measurements on liquid samples). Furthermore, the financial support of the Swiss National Science Foundation (project 200021-135496), the Nano-tera.ch Initiative (project SmartSphincter), the Danish Council for Independent Research, and the Swiss Nanoscience Institute (SNI) for their financial contribution to the AFM is gratefully acknowledged.

References

- [1] P. Chakraborti, H.A.K. Toprakci, P. Yang, N. Di Spigna, P. Franzone, T. Ghosh, A compact dielectric elastomer tubular actuator for refreshable Braille displays, *Sensors Actuators A Phys.* 179 (2012) 151–157.
- [2] R. Heydt, S. Chhokar, Refreshable braille display based on electroactive polymers, *Proc. Int. Disp. Res. Conf.* (2003) 5.
- [3] Z. Yu, W. Yuan, P. Brochu, B. Chen, Z. Liu, Q. Pei, Large-strain, rigid-to-rigid deformation of bistable electroactive polymers, *Appl. Phys. Lett.* 95 (2009) 192904.
- [4] L. Maffli, S. Rosset, M. Ghilardi, F. Carpi, H. Shea, Ultrafast all-polymer electrically tunable silicone lenses, *Adv. Funct. Mater.* 25 (2015) 1656–1665.
- [5] R. Heydt, R. Kornbluh, J. Eckerle, R. Pelrine, Sound radiation properties of dielectric elastomer electroactive polymer loudspeakers, *Proc. SPIE* 6168 (2006) (61681M-M-8).
- [6] I.A. Anderson, T.A. Gisby, T.G. McKay, B.M. O'Brien, E.P. Calius, Multi-functional dielectric elastomer artificial muscles for soft and smart machines, *J. Appl. Phys.* 112 (2012) 041101.
- [7] K. Gabor, L. Patrick, W. Michael, An arm wrestling robot driven by dielectric elastomer actuators, *Smart Mater. Struct.* 16 (2007) S306.
- [8] R. Pelrine, R.D. Kornbluh, Q. Pei, S. Stanford, S. Oh, J. Eckerle, et al., Dielectric elastomer artificial muscle actuators: toward biomimetic motion, *Proc. SPIE* 4695 (2002) 126–137.
- [9] K. Jung, K.J. Kim, H.R. Choi, A self-sensing dielectric elastomer actuator, *Sensors Actuators A Phys.* 143 (2008) 343–351.
- [10] M. Rosenthal, N. Bonwit, C. Duncheon, J. Heim, Applications of dielectric elastomer EPAM sensors, *Proc. SPIE* 6524 (2007) (65241F-F-7).
- [11] F. Carpi, D.D. Rossi, Improvement of electromechanical actuating performances of a silicone dielectric elastomer by dispersion of titanium dioxide powder, *IEEE Trans. Dielectr. Electr. Insul.* 12 (2005) 835–843.
- [12] G. Ouyang, K. Wang, X.Y. Chen, TiO₂ nanoparticles modified polydimethylsiloxane with fast response time and increased dielectric constant, *J. Micromech. Microeng.* 22 (2012) 074002.
- [13] G. Gallone, F. Galantini, F. Carpi, Perspectives for new dielectric elastomers with improved electromechanical actuation performance: composites versus blends, *Polym. Int.* 59 (2010) 400–406.
- [14] Z. Zhang, L. Liu, J. Fan, K. Yu, Y. Liu, L. Shi, et al., New silicone dielectric elastomers with a high dielectric constant, *Proc. SPIE* 6926 (2008) 692610–692618.
- [15] L. Jiang, A. Betts, D. Kennedy, S. Jerrams, Improving the electromechanical performance of dielectric elastomers using silicone rubber and dopamine coated barium titanate, *Mater. Des.* 85 (2015) 733–742.
- [16] P. Lotz, M. Matysek, P. Lechner, M. Hamann, H.F. Schlaak, Dielectric elastomer actuators using improved thin film processing and nanosized particles, *Proc. SPIE* 6927 (2008) (692723–10).
- [17] A. Egede Daugaard, S.S. Hassouneh, M. Kostrzewska, A.G. Bejenariu, A.L. Skov, High-dielectric permittivity elastomers from well-dispersed expanded graphite in low concentrations, *Proc. SPIE* 8687 (2013) (868729–11).
- [18] L. Chen, C. Liu, K. Liu, C. Meng, C. Hu, J. Wang, et al., High-performance, low-voltage, and easy-operable bending actuator based on aligned carbon nanotube/polymer composites, *ACS Nano* 5 (2011) 1588–1593.
- [19] L.Z. Chen, C.H. Liu, C.H. Hu, S.S. Fan, Electrothermal actuation based on carbon nanotube network in silicone elastomer, *Appl. Phys. Lett.* 92 (2008) 263104.
- [20] M. Molberg, D. Crespy, P. Rupper, F. Nüesch, J.-A.E. Månson, C. Löwe, et al., High breakdown field dielectric elastomer actuators using encapsulated polyaniline as high dielectric constant filler, *Adv. Funct. Mater.* 20 (2010) 3280–3291.
- [21] D.M. Opris, M. Molberg, C. Walder, Y.S. Ko, B. Fischer, F.A. Nüesch, New silicone composites for dielectric elastomer actuator applications in competition with acrylic foil, *Adv. Funct. Mater.* 21 (2011) 3531–3539.

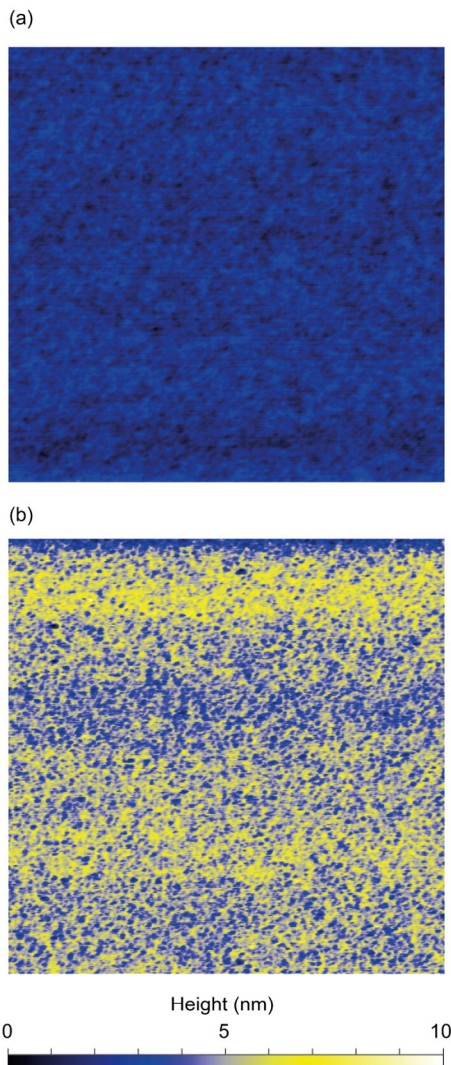


Fig. 6. AFM images of UV-cured surfaces for (a) DMS-V05 and (b) CI-PDMS. The scan size for both images is $5 \times 5 \mu\text{m}^2$. The surface roughness for the CI-PDMS film is more than twice the value of the DMS-V05 film.

- [22] B. Kussmaul, S. Risse, G. Kofod, R. Waché, M. Wegener, D.N. McCarthy, et al., Enhancement of dielectric permittivity and electromechanical response in silicone elastomers: molecular grafting of organic dipoles to the macromolecular network, *Adv. Funct. Mater.* 21 (2011) 4589–4594.
- [23] C. Racles, M. Cazacu, B. Fischer, D.M. Opris, Synthesis and characterization of silicones containing cyanopropyl groups and their use in dielectric elastomer actuators, *Smart Mater. Struct.* 22 (2013) 104004.
- [24] F.B. Madsen, A.E. Daugaard, S. Hvilsted, M.Y. Benslimane, A.L. Skov, Dipolar cross-linkers for PDMS networks with enhanced dielectric permittivity and low dielectric loss, *Smart Mater. Struct.* 22 (2013) 104002.
- [25] F.B. Madsen, L. Yu, A.E. Daugaard, S. Hvilsted, A.L. Skov, Silicone elastomers with high dielectric permittivity and high dielectric breakdown strength based on dipolar copolymers, *Polymer* 55 (2014) 6212–6219.
- [26] F.B. Madsen, I. Javakhishvili, R.E. Jensen, A.E. Daugaard, S. Hvilsted, A.L. Skov, Synthesis of telechelic vinyl/allyl functional siloxane copolymers with structural control, *Polym. Chem.* 5 (2014) 7054–7061.
- [27] F.B. Madsen, L. Yu, A.E. Daugaard, S. Hvilsted, A.L. Skov, A new soft dielectric silicone elastomer matrix with high mechanical integrity and low losses, *RSC Adv.* 5 (2015) 10254–10259.
- [28] T. Töpfer, F. Weiss, B. Osmani, C. Bippes, V. Leung, B. Müller, Siloxane-based thin films for biomimetic low-voltage dielectric actuators, *Sensors Actuators A Phys.* 233 (2015) 32–41.
- [29] D.A.G. Bruggeman, Berechnung verschiedener physikalischer Konstanten von heterogenen Substanzen. I. Dielektrizitätskonstanten und Leitfähigkeiten der Mischkörper aus isotropen Substanzen, *Ann. Phys.* 416 (1935) 665–679.
- [30] H. Fujiwara, J. Koh, P.I. Rovira, R.W. Collins, Assessment of effective-medium theories in the analysis of nucleation and microscopic surface roughness evolution for semiconductor thin films, *Phys. Rev. B* 61 (2000) 10832–10844.
- [31] P.J. Launer, Infrared Analysis of Organosilicon Compounds: Spectra-Structure Correlations, *Silicone Compounds Register and Review* 1987, p. 100.
- [32] F. Carpi, I. Anderson, S. Bauer, G. Frediani, G. Gallone, M. Gei, et al., Standards for dielectric elastomer transducers, *Smart Mater. Struct.* 24 (2015) 105025.
- [33] D. Gatti, H. Haus, M. Matysek, B. Frohnepfel, C. Tropea, H.F. Schlaak, The dielectric breakdown limit of silicone dielectric elastomer actuators, *Appl. Phys. Lett.* 104 (2014) 052905.
- [34] J. Huang, S. Shian, R.M. Diebold, Z. Suo, D.R. Clarke, The thickness and stretch dependence of the electrical breakdown strength of an acrylic dielectric elastomer, *Appl. Phys. Lett.* 101 (2012) 122905.
- [35] M. Kollosche, H. Stoyanov, H. Ragusch, S. Risse, A. Becker, G. Kofod, Electrical Breakdown in Soft Elastomers: Stiffness Dependence in Un-pre-stretched Elastomers, 2010 10th IEEE Int. Conf. Solid Dielectr 2010, pp. 1–4.
- [36] S. Vudayagiri, S. Zakaria, L. Yu, S.S. Hassouneh, M. Benslimane, A.L. Skov, High breakdown-strength composites from liquid silicone rubbers, *Smart Mater. Struct.* 23 (2014) 105017.
- [37] L. Yu, S. Vudayagiri, S. Zakaria, M.Y. Benslimane, A.L. Skov, Filled liquid silicone rubbers: possibilities and challenges, *Proc. SPIE* 9056 (2014) (90560S-S-9).
- [38] S.J. Clarson, J.A. Semlyen, *Siloxane Polymers*, Prentice Hall, 1993.
- [39] B. Schnyder, T. Lippert, R. Köttz, A. Wokaun, V.-M. Graubner, O. Nuyken, UV-irradiation induced modification of PDMS films investigated by XPS and spectroscopic ellipsometry, *Surf. Sci.* 532–535 (2003) 1067–1071.
- [40] L.M. Landsberger, W.A. Tiller, Refractive index, relaxation times and the viscoelastic model in dry-grown SiO₂ films on Si, *Appl. Phys. Lett.* 51 (1987) 1416–1418.
- [41] S.N. Yahya, C.K. Lin, M.R. Ramli, M. Jaafar, Z. Ahmad, Effect of cross-link density on optoelectronic properties of thermally cured 1,2-epoxy-5-hexene incorporated polysiloxane, *Mater. Des.* 47 (2012) 416–423.
- [42] K.L. Johnson, K. Kendall, A.D. Roberts, Surface energy and the contact of elastic solids, *Proc. R. Soc. Lond. A* 324 (1971) 301–313.
- [43] H.-J. Butt, B. Cappella, M. Kappl, Force measurements with the atomic force microscope: technique, interpretation and applications, *Surf. Sci. Rep.* 59 (2005) 1–152.
- [44] H.-C. Kim, T.P. Russell, Contact of elastic solids with rough surfaces, *J. Polym. Sci. B Polym. Phys.* 39 (2001) 1848–1854.
- [45] P. Sommer-Larsen, A.L. Larsen, Materials for dielectric elastomer actuators, *Proc. SPIE* 5385 (2004) 68–77.